Influence of Sample Gas Humidity on Product Ion Formation in High Kinetic Energy Ion Mobility Spectrometry (HiKE-IMS)

Christoph Schaefer*, Florian Schlottmann, Ansgar T. Kirk, Stefan Zimmermann

Leibniz University Hannover, Institute of Electrical Engineering and Measurement Technology, Department of Sensors and Measurement Technology, Appelstr. 9A, 30167 Hannover, Germany

*Corresponding author: schaefer@geml.uni-hannover.de

Keywords: high kinetic energy ion mobility spectrometry; ion mobility spectrometry; ionization; moisture; humidity

Abstract

High Kinetic Energy Ion Mobility Spectrometers (HiKE-IMS) chemically ionize gaseous samples via reactant ions and separate the generated ions by their motion in a neutral gas under the influence of an electric field. Operation at reduced pressures of 10 – 40 mbar allows for reaching high reduced electric field strengths (*E*/*N*) of up to 120 Td. At these high *E*/*N*, the generated ions gain the namesake high kinetic energies, leading to a decrease in cluster size of the reactant ions by increasing the reaction rate of collision-induced cluster dissociation of hydrates. In positive ion polarity and in purified air, $H_3O^+(H_2O)_n$, $NO^+(H_2O)_n$, and $O_2^{+\bullet}(H_2O)_p$ are the most abundant reactant ions. In this work, we investigate the effect of varying sample gas humidity on product ion formation for several model substances. Results show that increasing the sample gas humidity at high *E*/*N* of 120 Td shifts product ion formation from a charge transfer dominated reaction system to a proton transfer dominated reaction system. For HiKE-IMS operated at high *E*/*N*, the reduction in cluster size of reactant ions allows ionization of analytes with low proton affinity even at high relative humidity in the sample gas of RH = 75% at 303.15 K and 1013.25 hPa. In contrast to conventional IMS, where increasing the sample gas humidity inhibits ionization for various analytes, increasing sample gas humidity in HiKE-IMS operated at 120 Td is actually beneficial for ionization yield of most analytes investigated in this work as it increases the number of $H_3O^+(H_2O)_n$.

Introduction

Ion mobility spectrometers (IMS) separate ions in a drift region by their motion in a neutral drift gas under the influence of an electric field. Often, IMS use primary ionization methods such as corona discharge or β-radiation from ^{63}Ni or ^{3}H to generate reactant ions that subsequently ionize neutral analyte molecules in a reaction region via different gas-phase reactions.[1,2] Due to the large number of ion-neutral collisions at ambient pressure, IMS can achieve low limits of detection down to the single-digit ppt_V (parts-per-trillion by volume) range in short measurement times of less than 1 s.[3]

When operated in positive ion polarity with purified air, the above ionization sources initially form primary ions such as $N_2^{+\bullet}$, $O_2^{+\bullet}$, and NO^+.[4–7] However, given the large amount of neutral oxygen molecules in air, $N_2^{+\bullet}$ rapidly reacts with O_2 by charge transfer to form $O_2^{+\bullet}$.[5] Furthermore, in the presence of trace amounts of water, $N_2^{+\bullet}$ reacts in a reaction cascade to form hydrated hydronium ions $H_3O^+(H_2O)_n$.[4,5] The other primary ions NO^+ and $O_2^{+\bullet}$ formed in the ion source form the unstable hydrates $NO^+(H_2O)_3$ and $O_2^{+\bullet}(H_2O)$, which ultimately form hydrated hydronium ions upon reactions with other neutral water molecules and are therefore not detected.[5,8–11] $NO^+(H_2O)_m$ is present and can thus serve as a reactant ion only at very low water volume fractions of less than or equal to 1 ppm_V.[12,13] Therefore, $H_3O^+(H_2O)_n$ are the most abundant reactant ions with a typical cluster size between n = 2 and n = 3 at a water volume fraction of 1 ppm_V[14] in IMS operated at ambient pressure.[1,14] As the water volume fraction inside IMS increases, the cluster size n of the reactant ions also increases, inhibiting the ionization of nonpolar analytes with low proton affinity (PA). For example, publications in the literature

report inhibited ionization of alcohols and aldehydes at water volume fractions above 100 ppm_V and an operating temperature of 323 K,[15] and strongly reduced signal intensities of ketones, e.g. 2-butanone, and aromatic hydrocarbons above water volume fractions of several 100 ppm_V.[14] Although the low limits of detection render IMS a versatile tool for the detection of organic compounds, IMS suffer from a limited ionization yield for several analytes and a strong dependence of ionization on humidity.[14–18]

Unlike conventional IMS for trace gas analysis, which operate at ambient pressure, High Kinetic Energy Ion Mobility Spectrometers (HiKE-IMS) operate at a reduced pressure of 10 – 40 mbar allowing for high reduced electric field strengths (E/N) of up to 120 Td (1 Td = $1 \cdot 10^{-21}$ $V \cdot m^2$).[19–21] For comparison, in IMS that operate at ambient pressure, E/N typically does not exceed 2 Td.[22,23] HiKE-IMS consist of a reaction region to ionize gaseous samples and a drift region to separate the generated ions by their ion mobility. Typically, a corona discharge ionization source ionizes the main constituents of the neutral gas present in the HiKE-IMS, initiating the formation of the reactant ions $H_3O^+(H_2O)_n$, $NO^+(H_2O)_m$, and $O_2^{+\bullet}(H_2O)_p$ in positive ion polarity using purified air as neutral gas with water volume fractions below 4200 ppm_V.

In HiKE-IMS, E/N is one of the most important parameters as it determines the effective temperature T_{eff}[24] of a gas-phase ion and thus significantly affects the ion's kinetic energy. By operating HiKE-IMS at high E/N, the ions reach high kinetic energies, causing collision-induced cluster dissociation of ion-neutral clusters such as hydrates of the reactant ions.[25–27] Previous studies on the influence of E/N and humidity on reactant ion population in HiKE-IMS have shown that the cluster size of reactant ions decreases with increasing E/N.[28,29] Consequently, operation of HiKE-IMS at high E/N results in collision-induced cluster dissociation of the hydrates $NO^+(H_2O)_m$ and $O_2^{+\bullet}(H_2O)_p$ preventing their conversion to hydrated hydronium ions when the cluster sizes decrease below the critical cluster sizes $m = 3$ and $p = 1$. Additionally, increasing E/N reduces the residence time of the ion in the reaction region, which, combined with the decreased number of collisions at the reduced operating pressure, allows thermodynamically unfavorable ion species (ions that would not be present or less abundant when the reaction system reaches thermodynamic equilibrium) to be maintained for a longer time. For example, the protonated monomer of benzene can be detected in HiKE-IMS in the presence of toluene and xylene both of which have a higher PA than benzene.[30] Thus, as E/N increases, the reaction system in HiKE-IMS transitions from thermodynamic control, where the ion population is determined by the thermodynamic properties of the neutral analytes and reactant ions and thus the analytes with the highest PA or the lowest ionization energy (IE) are ionized and detected, to kinetic control, where the ion population is determined by the kinetics of the gas-phase reactions between the reactant ions and the neutral analytes and thermodynamic equilibrium is not established due to insufficient reaction time. Besides E/N, the water volume fraction also affects the cluster size of a hydrated ion: on the one hand, as E/N increases, more hydrates dissociate as the reaction rate of cluster dissociation increases. On the other hand, as water volume fraction decreases, fewer hydrates are formed as the reaction rate of cluster association decreases. Thus, both an increase in E/N and a decrease in water volume fraction lead to smaller cluster size of hydrated gas-phase ions.[25,29]

Previous publications have explained the ion-neutral reactions involved in product ion formation in HiKE-IMS in detail.[31] Here we summarize only the aspects of product ion formation that are important for this work. In HiKE-IMS, an analyte M can react with $H_3O^+(H_2O)_n$ via proton transfer and ligand switching reactions forming the protonated monomer and its hydrates $MH^+(H_2O)_x$ with a typical cluster size between $x = 0$ and 2. If the proton affinity of the analyte exceeds that of the corresponding neutral water cluster $(H_2O)_{n+1}$, proton transfer is exothermic.[32] For ligand switching, the reaction enthalpy depends on the PA of both the water monomer H_2O and the analyte M as well as on the hydration enthalpy of the respective reactant ion and the protonated monomer MH^+. Ligand switching with hydrated hydronium ions becomes more exothermic for analytes having a high PA and high hydration

enthalpy.[16,31] The collision-induced cluster dissociation of $H_3O^+(H_2O)_n$ forming the bare H_3O^+ at high *E*/*N* allows the ionization of nonpolar analytes with low proton affinity above the proton affinity of water of 691 kJ/mol via proton transfer.[33,34]

Besides hydrated hydronium ions, the reactant ions $NO^+(H_2O)_m$ and $O_2^{+\bullet}(H_2O)_p$ may constitute a significant fraction of the reactant ion population in HiKE-IMS and are thus involved in product ion formation via charge transfer and adduct formation.[30,31] If an analyte has lower IE than the neutral precursors of the reactant ions with IE(NO) = 9.26 eV and IE(O_2) = 12.06 eV,[34] charge transfer with NO^+ and $O_2^{+\bullet}$ forming the precursor radical cation $M^{+\bullet}$ is exothermic. Since O_2 has comparatively high ionization energy, charge transfer involving $O_2^{+\bullet}$ can lead to fragmentation of the neutral analyte molecules.[35,36] Similar to the hydration of H_3O^+, the hydration of NO^+ and $O_2^{+\bullet}$ can also inhibit ionization of analytes via charge transfer since it reduces the effective recombination energy by the binding energy of NO^+ and $O_2^{+\bullet}$ to H_2O.[37] Therefore, the ability of HiKE-IMS to control the cluster size of reactant ions, and thus the ability to ionize and detect analytes that cannot be ionized efficiently at ambient pressure, especially at high sample gas humidity, may compensate for the lower sensitivity of HiKE-IMS caused by the lower number of ion-neutral collisions compared to IMS operated at ambient pressure. Furthermore, the reduced number of collisions in HiKE-IMS also reduces chemical cross-sensitivities, making HiKE-IMS a suitable tool e.g. for the detection of TICs.[38] To improve the sensitivity of HiKE-IMS to reach detection limits even in the low ppb_V range while maintaining high *E*/*N* allowing the bare H_3O^+ and $O_2^{+\bullet}$ to ionize analytes, the operating pressure of HiKE-IMS can be increased up to 40 mbar, as shown in previous publications.[21]

Some physicochemical properties of the neutral species, especially the vapor pressure, as well as the melting point and boiling point, can affect the detection of these analytes in (HiKE-)IMS, since they decide whether neutral molecules are present in the gas-phase in amounts sufficient for their detection. However, once the analyte molecules are present in the reaction region of HiKE-IMS, the thermodynamic properties of the neutral molecule and the reactant ions determine the ionization of these analytes.

In HiKE-IMS, a single analyte can form multiple product ions due to the numerous possible reaction pathways involving the different reactant ions, increasing the complexity of product ion formation compared to conventional IMS, where mainly the (hydrated) protonated monomer and the proton-bound dimer are formed.[22] For example, aromatic hydrocarbons can form the protonated monomer and the precursor radical cation in positive ion polarity with their abundances depending on *E*/*N* and humidity,[31,33] whereas H_2S can form up to three different product ions in negative ion polarity.[38] Previous publications have investigated the influence of *E*/*N* on product ion formation in HiKE-IMS for various analytes.[31,33] However, detailed studies on the influence of humidity on product ion formation in HiKE-IMS are still missing. In this work, we, therefore, investigate the influence of sample gas humidity on the product ion formation of several model substances in positive ion polarity using HiKE-IMS. In this context, we address which product ions are formed, and which reactant ions are involved in their formation. In particular, the reactions between the analytes and the hydrated reactant ions are studied depending on their cluster size. Furthermore, since the strong influence of humidity on the cluster size of reactant ions, as known from conventional IMS, should be reduced in HiKE-IMS operating at high *E*/*N*, the negative influence of increased sample gas humidity on signal intensity and thus sensitivity should be mitigated. To validate the ability of HiKE-IMS to ionize analytes even at high sample gas humidity, we investigate the ionization yield at varying water volume fractions in the sample gas between 70 ppm_V and relative humidity of RH = 75% at 303.15 K and 1013.25 hPa for benzene, pyridine, acetone, 2-butanone, methanol, and 1-propanol.

Experimental

To investigate the effect of sample gas humidity on the formed product ions, the HiKE-IMS is coupled to a time-of-flight mass spectrometer (TOF-MS) as shown in Figure 1.[28] In general, the HiKE-IMS-MS consists of three main parts: (1) the HiKE-IMS, (2) a transfer stage, and (3) a self-built TOF-MS. As mentioned in the Introduction, a corona discharge ionization source in point-to-plane geometry is used to initiate reactant ion formation. The formed reactant ions then ionize neutral analytes within the reaction region. A tristate ion shutter[39] gates the entire ion population consisting of reactant ions and product ions that is present at the end of the reaction region into the drift region, where the ions are separated by their ion mobility. Another ion gate at the end of the drift region controls the transmission of ions into the transfer stage. The HiKE-IMS, operated at a pressure of 14.3 mbar, is separated from the transfer stage by a pinhole with a diameter of 0.8 mm. The transfer stage consists of two sections with different operating pressures: a first section operating at $6 \cdot 10^{-3}$ mbar and a second section operating at $6 \cdot 10^{-6}$ mbar, separated by a skimmer with a hole diameter of 1 mm located at a distance of 20 mm from the first pinhole. After passing through the skimmer, the ions are directed into the TOF-MS by an Einzel lens consisting of three stainless steel ring electrodes with an inner diameter of 19 mm each and a distance of 15 mm, separated by polyether ether ketone (PEEK) spacers. The TOF-MS also operates at a pressure of $6 \cdot 10^{-6}$ mbar. Detailed information on the used HiKE-IMS and the TOF-MS can be found in a previous publication by Allers et al.[28] Since the quadrupole ion guide that was previously used in the transfer stage as described by Allers et al. significantly manipulated the ion population by cluster dissociation, it was exchanged by the transfer stage described above. All experiments presented in the main manuscript are conducted in the *Continuous-Ion-Flow mode*, where both ion gates are left open to continuously transfer the formed ions into the TOF-MS.

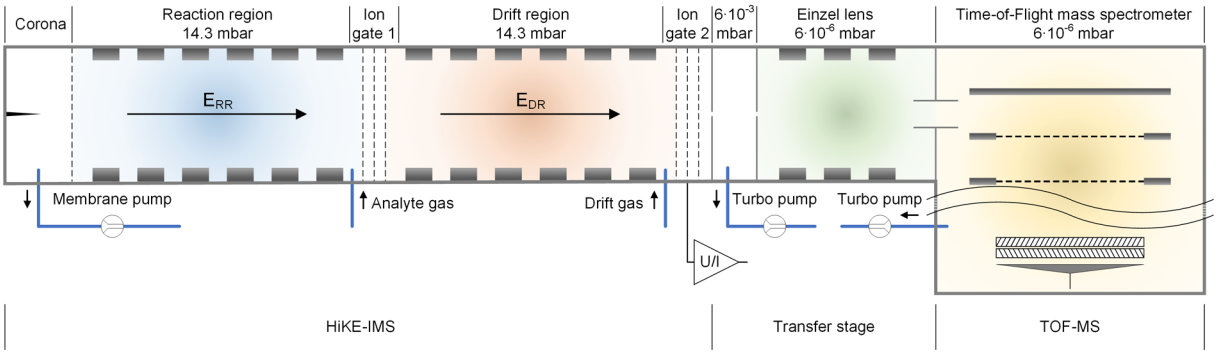

Figure 1. Schematic of the HiKE-IMS-MS.

Table 1 summarizes the most important operating parameters of the used HiKE-IMS. The reduced reaction field strength E_{RR}/N influences both reactant ion formation and product ion formation as it controls the field-dependent cluster size of the reactant ions. The reduced drift field strength E_{DR}/N affects the separation of different ion species within the drift region. However, the reduced drift field strength also controls the cluster size of the ions within the drift region and can cause field-induced fragmentation of the product ions. To ensure comparable conditions in both regions, the reduced electric field strength in both the reaction region and the drift region is set to the same value in all experiments of this work.

Table 1. Operating parameters of the HiKE-IMS. Gas flow rates correspond to reference conditions 293 K and 1013.25 hPa.

Parameter	Value
reaction region length	105 mm
drift region length	153,5 mm
drift region diameter	21 mm
corona voltage	1050 V

reaction region voltage	1,5 - 4 kV
drift region voltage	2,5 - 6 kV
reduced reaction and reduced drift field, *E*/*N*	50 - 120 Td
injection time	1 µs
drift gas flow, Q_{DG}	24 ml_s/min
sample gas flow, Q_{SG}	15 ml_s/min
operating pressure	14.3 mbar
operating temperature	30°C
dew point of the drift gas	-50°C (70 ppm_V)
Ion residence times in reaction region at 50 Td	300 - 450 µs
Ion residence times in reaction region at 120 Td	100 - 160 µs
Ion residence times in drift region at 50 Td	450 - 680 µs
Ion residence times in drift region at 120 Td	150 - 240 µs

All chemicals were purchased from Sigma-Aldrich Germany with a purity of ≥ 99 % and used without further purification. A zero-air generator (JAGZAG600S, JAG, Germany) combined with a pressure swing absorber (CAS1, PureGas, Germany) in series with an additional moisture trap (Molecular Sieve 5A Moisture Trap, Supelco, USA) and an activated carbon filter (Supelcarb® HC Hydrocarbon Trap, Supelco, USA) supplies purified air containing < 1 ppm_V of water as drift gas. As shown in Figure S1, samples were introduced using a heated sample container (T = 35 °C) and homemade permeation tubes. Water volume fraction in the sample gas can be varied by mixing the provided purified air containing < 1 ppm_V of water with purified air passed through a water container. Using this method, a maximum water volume fraction in the sample gas of ϕ_{H2O} = 32000 ppm_V can be reached, corresponding to a relative sample gas humidity (RH) of RH = 75 % at a temperature of 303.15 K and 1013.25 hPa. To keep the volume fraction of analytes in the sample gas constant, the total flow rate of the sample gas passing through the sample container is kept constant at 300 ml_s/min (milliliter standard per minute, mass flow at reference conditions 293 K and 1013.25 hPa). Therefore, when changing the mixing ratio of dry and humidified air, the absolute flow rates of dry and humid air are set accordingly. The sample gas is transferred into the HiKE-IMS via a capillary with 250 µm inner diameter adapted to a stainless steel T-piece. The capillary serves as flow restriction and its length is adjusted to provide a gas flow rate of 15 ml_s/min. A mass flow controller (F-200DV-ABD, Bronkhorst Nord GmbH, Germany) supplies the drift gas with a gas flow rate of 24 ml_s/min. Dew point sensors (Easidew Transmitter, Michell Instruments, Germany) measure the resulting water volume fraction of both sample and drift gas. Due to diffusion through seals and PTFE tubings, the residual water volume fraction may well exceed 1 ppm_V. To ensure comparability of the results, we intentionally increased the water volume fraction in both sample and drift gas to ϕ_{H2O} = 70 ppm_V, which is referred to as dry conditions below.

As described in previous publications,[28,39] the gas outlet for evacuating the HiKE-IMS is located at the corona discharge ionization source in the reaction region on the opposite side of the ion gate. As a consequence, sample and drift gas dilute within the reaction region. Thus, when the sample gas humidity is increased, the water volume fraction inside the reaction region will be lower than in the sample gas as the water volume fraction in the drift gas remains constant at 70 ppm_V. Since the sample gas should not enter the drift region, the drift gas is not diluted and the water volume fraction in the drift region remains constant at 70 ppm_V whilst varying sample gas humidity. Thus, in the following sections, the water volume fraction in the sample gas is given instead of the water volume fraction inside the reaction region. Assuming ideal mixing of sample and drift gas within the reaction region, the water volume fraction ϕ_{H2O} inside the reaction region can be calculated according to eq. 1 with $\phi_{H2O,SG}$ and $\phi_{H2O,DG}$ being the water volume fraction inside the sample and drift gas, respectively, Q_{SG} being the sample gas flow rate, and Q_{DG} being the drift gas flow rate.

$$\phi_{H2O} = \frac{\phi_{H2O,SG} \cdot Q_{SG} + \phi_{H2O,DG} \cdot Q_{DG}}{Q_{SG} + Q_{DG}} \quad (1)$$

Results and Discussion

For the experiments shown in this work, it is important to ensure that ion transmission between HiKE-IMS and TOF-MS does not depend on ion mass. To verify that ion transmission is independent of ion mass, ion mobility spectra of acetone and 2-butanone were first recorded in *IMS-Only mode* at two fixed E_{DR}/N of 60 Td and 120 Td, while varying E_{RR}/N between 60 Td and 120 Td in steps of 1 Td. The *Selected-Mobility mode*, in which the tristate ion shutter located at the end of the drift region just transfers selected regions of the ion mobility spectra into the TOF-MS, was used to identify the ion species underlying the transferred peaks in the ion mobility spectra with the TOF-MS. The ion mobility spectra and mass spectra of acetone and 2-butanone in both the reaction region and the drift region are shown in Figures S2 and S3, respectively. Furthermore, the same sweep of reduced electric field strength in the reaction region was repeated in the *Continuous-Ion-Flow mode*, where both ion gates are open to transfer all formed ions into the TOF-MS. The comparison of the relative abundances of the ions determined in *IMS-Only mode* with those determined in *Continuous-Ion-Flow mode* shown in Figures S4-S7 is within error limits for both acetone and 2-butanone in all experiments, suggesting that ion transmission in HiKE-IMS-MS does not depend on ion mass for the mass range relevant in this work.

To investigate the influence of sample gas humidity on product ion formation in HiKE-IMS in positive ion polarity mode, mass spectra are recorded at two fixed E/N of 50 Td and 120 Td, with equal E/N in both the reaction and drift region, while varying water volume fraction from dry conditions with ϕ_{H2O} = 70 ppm_V up to ϕ_{H2O} = 32000 ppm_V corresponding to RH = 75% at 303.15 K and 1013.25 hPa. Comparing the experiment at a high E/N of 120 Td with the experiment at an intermediate E/N of 50 Td shows the influence of different cluster sizes of the reactant ions on product ion formation. First, blank measurements without adding analytes to the sample gas are conducted to determine the respective reactant ion population. Subsequently, the measurements were repeated by adding each analyte individually to the sample gas with a volume fraction of 2 ppm_V. To verify reproducibility, each measurement was repeated ten times.

Reactant Ion Population Depending on Sample Gas Humidity

Figure 2 shows the recorded mass spectra using purified air without any analytes in the sample gas at three different water volume fractions inside the sample gas and constant E/N of 120 Td in both the reaction region and the drift region. Multiple ion species with their abundance depending on sample gas humidity are detected in these blank measurements. As expected, the reactant ions H_3O^+ (m/z 19), NO^+ (m/z 30), and $O_2^{+\bullet}$ (m/z 32) are the most abundant ion species. An additional ion species with m/z 64 is detected at low sample gas humidity when $O_2^{+\bullet}$ is present, which might be an adduct of $O_2^{+\bullet}O_2$ with neutral oxygen molecules.[5] Another ion species with m/z 47 is detected at high sample gas humidity when H_3O^+ is the most abundant ion species. We suspect that this is an adduct of $H_3O^+N_2$ with neutral nitrogen. Similar adducts of the hydrated hydronium ions with N_2 have been found in an IMS operated at ambient pressure coupled to a mass spectrometer.[40] Since both adducts $O_2^{+\bullet}O_2$ and $H_3O^+N_2$ can rapidly undergo ligand switching with H_2O that would prevent their detection,[41] the adducts presumably form when $O_2^{+\bullet}$ and H_3O^+ enter the transfer stage between the IMS and the TOF-MS.

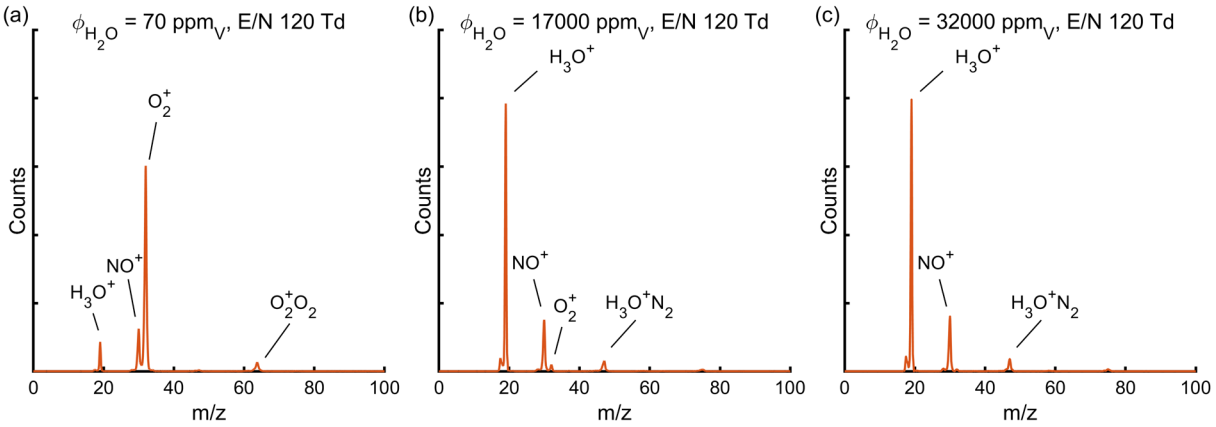

Figure 2: Mass spectra in positive ion polarity using purified air without any analytes in the sample gas at three different water volume fractions in the sample gas of (a) ϕ_{H2O} = 70 ppm$_V$, (b) ϕ_{H2O} = 17000 ppm$_V$, and (c) ϕ_{H2O} = 32000 ppm$_V$ at E/N = 120 Td in both the reaction region and the drift region. Table 1 summarizes all other operational parameters.

As the mass spectra show, the abundances of the reactant ions, particularly that of H_3O^+ and $O_2^{+\bullet}$, are strongly affected by sample gas humidity. While at ϕ_{H2O} = 70 ppm$_V$, $O_2^{+\bullet}$ is the most abundant reactant ion, at a water volume fraction of ϕ_{H2O} = 32000 ppm$_V$, H_3O^+ is the dominant reactant ion, and $O_2^{+\bullet}$ is no longer detected. The influence of sample gas humidity on the reactant ion population is evident from the relative abundances of the reactant ions detected in the blank measurements as shown in Figure 3. Relative abundances were determined by normalizing the peak area of a specific ion to the integral of the mass spectrum, thus reflecting the proportion of the ion in the total ion population. When increasing the water volume fraction in the sample gas at *E*/*N* = 120 Td as shown in Figure 3 (b), the relative abundance of $O_2^{+\bullet}$ decreases, and the relative abundance of H_3O^+ increases. Possibly, $O_2^{+\bullet}$ temporarily forms the unstable monohydrate, which is then converted to hydrated hydronium ions when reacting with neutral water molecules. In contrast, the relative abundance of NO^+ remains constant at 20 % of the total ion population independent of sample gas humidity. Due to collision-induced cluster dissociation, the monohydrates of H_3O^+ and NO^+ are not detected at *E*/*N* = 120 Td. At such *E*/*N*, the HiKE-IMS is operated at sufficiently high reduced electric field strength to ensure that the bare reactant ions are present instead of their hydrates.

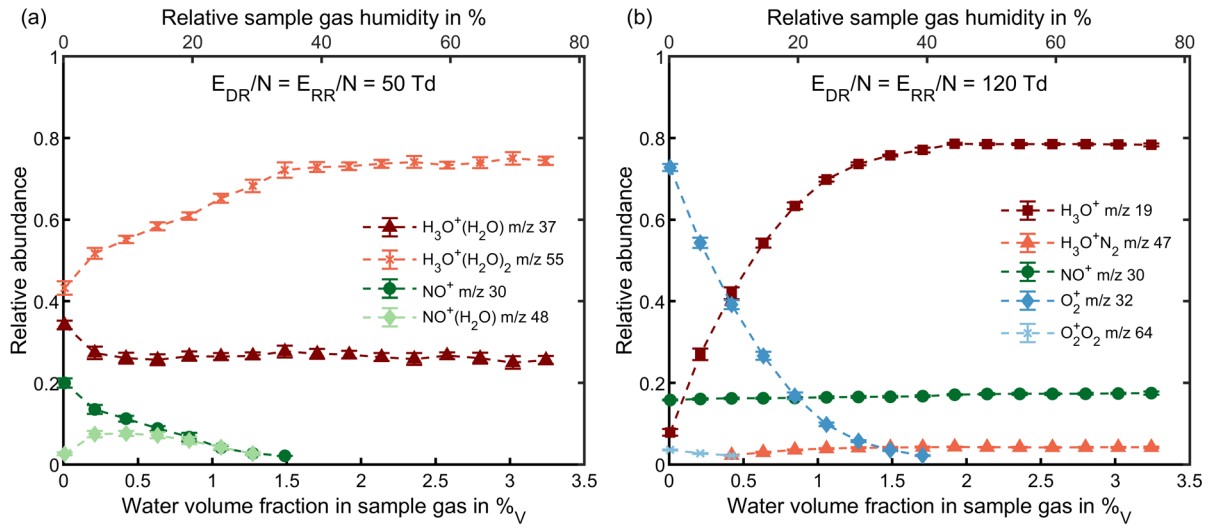

Figure 3. Reactant ion population in HiKE-IMS-MS in positive ion polarity using purified air without any analytes in the sample gas depending on water volume fraction in the sample gas. (a) Relative abundances of reactant ions at a reduced electric field strength of 50 Td. (b) Relative abundances of reactant ions at a reduced electric field strength of 120 Td. The relative abundances are determined by normalizing the peak integral of the specific reactant ion to the total integral of the mass spectrum. The relative humidity of the sample gas refers to 303.15 K and 1013.25 mbar. All other parameters are listed in Table 1. The error bars show the standard deviation of ten individual measurements.

When decreasing reduced electric field strength from high E/N of 120 Td to intermediate E/N of 50 Td, the reactant ion population changes for two reasons: First, due to the lower kinetic energy of the reactant ions at 50 Td, the reaction rate of cluster dissociation decreases, and therefore the reactant ions form larger hydrates. Second, the reaction time is prolonged as the drift velocities of the ions decrease in both reaction region and drift region, so that thermodynamically unfavorable states cannot be maintained. As a result, $O_2^{+\bullet}$ cannot be detected at E/N = 50 Td even at the lowest water volume fraction of ϕ_{H2O} = 70 ppm_V. Instead, mainly $H_3O^+(H_2O)_n$ with n = 1 and n = 2 and to a lesser extent NO^+ and its monohydrate can be detected. When increasing the water volume fraction at E/N = 50 Td, the relative abundance of $NO^+(H_2O)_m$ with m = 0 and m = 1 decreases, since the unstable cluster $NO^+(H_2O)_3$ is formed, which reacts with neutral water molecules to form $H_3O^+(H_2O)_n$. Therefore, due to the lower reaction rate of cluster dissociation and the prolonged reaction times compared to the operation at 120 Td, the reduced electric field strength of 50 Td cannot prevent the conversion of $NO^+(H_2O)_m$ to hydrated hydronium ions and hence only $H_3O^+(H_2O)_n$ with n = 1 and n = 2 are detected at high water volume fractions above ϕ_{H2O} = 15000 ppm_V corresponding to RH = 35 % at 303.15 K and 1013.25 hPa. It should be noted that the cluster size determined by the TOF-MS does not necessarily correspond to the cluster size of the reactant ions in the reaction region due to possible cluster dissociation in the transfer stage. The implications of the changes in reactant ion population with sample gas humidity for product ion formation in HiKE-IMS are shown below for several model substances.

Product Ion Formation Depending on Sample Gas Humidity

Table 2 summarizes the analytes investigated in this work and their properties relevant for ionization, such as IE, PA, and hydration enthalpy ΔH_{Hyd} of the protonated monomer. Reaction enthalpies for proton transfer, ligand switching, and charge transfer based on the properties shown in Table 2 are summarized in the Supporting Information in Tables S1-S3. For all analytes, the hydration enthalpies ΔH_{Hyd} of the protonated monomer are known from the literature,[42–44] allowing calculation of the reaction enthalpy of ligand switching forming $MH^+(H_2O)$. The data show that for benzene, ligand switching via $H_3O^+(H_2O)_n$ with $n \geq 1$ is endothermic, and only proton transfer with the bare H_3O^+ is exothermic. For all other analytes, ligand switching with $H_3O^+(H_2O)$ forming the monohydrate of the protonated monomer is exothermic. In addition, due to the high IE of O_2, the charge transfer with $O_2^{+\bullet}$ is exothermic for all analytes. However, as discussed in the Introduction, the large difference in ionization energy between O_2 and the analytes might cause fragmentation of the product ions. In contrast, ionization via charge transfer with NO^+ is only exothermic for benzene and thermoneutral for pyridine. If NO^+ forms the monohydrate via hydration, charge transfer with benzene and pyridine also becomes endothermic.

Table 2. Gas-phase ion energetics data for the investigated analytes and the neutral precursors of the reactant ions, taken from the NIST Chemistry WebBook.[34] [a] Proton affinities of neutral water clusters $(H_2O)_n$ were taken from reference [45] [b] Hydration enthalpy of MH^+ of benzene was taken from reference [42]. [c] Hydration enthalpies of MH^+ of methanol and 1-propanol were taken from reference [43]. [d] Hydration enthalpies of MH^+ of the remaining analytes were taken from reference [44].

Compound	Molar mass in g/mol	IE in eV	PA in kJ/mol	$\Delta H_{Hyd}(MH^+)$ in kJ/mol
H_2O	18.015	12.62	691	-136
$(H_2O)_2$	36.031		832.7[a]	-84
$(H_2O)_3$	54.046		888.6[a]	-73
$(H_2O)_4$	72.061		919.5[a]	-56
$(H_2O)_5$	90.076		926.3[a]	-50
NO	30.006	9.26	531.8	
O_2	31.999	12.07	421	
Benzene	78.112	9.24	750.4	-71[b]
Pyridine	79.099	9.26	930	-66.5[d]
Acetone	58.079	9.7	812	-91.9[d]
2-butanone	72.106	9.52	827.3	-85.6[d]

Methanol	32.042	10.84	754.3	-115.6[c]
1-propanol	60.095	10.22	786.5	-100.1[c]

Product Ion Formation at 50 Td

Figures 4 and 5 show the product ion fractions of all investigated analytes at both E/N = 50 Td and 120 Td, which were determined by normalizing the peak areas of the specific product ion to the total peak areas of all product ions formed by the specific analyte. First, the results of the experiment at E/N = 50 Td for the various analytes forming multiple product ions will be considered, with $H_3O^+(H_2O)_n$ being the most abundant reactant ions. Accordingly, the reaction pathways involving the hydrated hydroniums ions dominate, namely proton transfer, ligand switching, and subsequent dimer formation. Therefore, the protonated monomer along with its hydrates and proton-bound dimers are the most abundant product ions at 50 Td. As the only exception, benzene does not form the protonated monomer at 50 Td, since ligand switching and proton transfer with the hydrates of H_3O^+ present under these conditions are endothermic. The results also show that the analytes having a higher hydration enthalpy of the protonated monomer form hydrates $MH^+(H_2O)_x$ with larger cluster sizes x since hydration is energetically more favorable. Correspondingly, methanol and 1-propanol form the mono- and dihydrate of MH^+ under these conditions, while acetone and 2-butanone only form the monohydrate, and pyridine does not form any hydrate of MH^+. While the reaction pathways involving $H_3O^+(H_2O)_n$ dominate at 50 Td, additional reaction channels involving NO^+, such as charge transfer and adduct formation, can form the precursor radical cation $M^{+\bullet}$ and the adduct MNO^+, especially at water volume fractions below ϕ_{H2O} = 15000 ppm_V corresponding to RH = 35 % at 303.15 K and 1013.25 hPa. Correspondingly, benzene and pyridine can form the precursor radical cation $M^{+\bullet}$ via charge transfer with NO^+ at 50 Td. All other analytes do not react with NO^+ via charge transfer, since the reaction is endothermic. In addition, all investigated analytes except for 1-propanol form the adduct MNO^+. Instead, 1-propanol forms an ion with m/z 77, which possibly is the hydrate of the ion $(M\text{-}H)^+$ formed via hydride ion abstraction of the parent molecule, which will be discussed in more detail below.

When increasing the water volume fraction, NO^+ is gradually converted to hydrated hydronium ions $H_3O^+(H_2O)_n$. Accordingly, the fractions of the product ions formed by NO^+ decrease. Although NO^+ is not detected at the highest water volume fraction of ϕ_{H2O} = 32000 ppm_V corresponding to RH = 75% at 303.15 K and 1013.25 hPa, it is still present in parts of the reaction region, especially near the corona needle where reactant ion formation is initiated. Thus, when NO^+ drifts through the reaction region and is slowly converted to hydrated hydronium ions, it can still be involved in product ion formation. Correspondingly, the precursor radical cations $M^{+\bullet}$ of pyridine and benzene, as well as the adduct MNO^+ of benzene, can still be detected at the maximum water volume fraction of ϕ_{H2O} = 32000 ppm_V. For all analytes except for benzene, the decreasing product ion fraction of the product ions associated with NO^+ causes the product ion fractions of the product ions formed by $H_3O^+(H_2O)_n$ to increase. As explained above, benzene does not react with the hydrates of H_3O^+ that are present at 50 Td. Especially in the case of methanol and 1-propanol, the product ion fractions of $MH^+(H_2O)$ increase accompanied by a simultaneous decrease in the product ion fractions of the proton-bound dimers. Possibly, hydration is more likely than dimer formation when the water volume fraction inside the reaction region increases. In summary, at intermediate E/N of 50 Td, the reaction system in HiKE-IMS is still dominated by the reactions with $H_3O^+(H_2O)_n$, similar to that in conventional IMS, and thus mainly the (hydrated) protonated monomers and the proton-bound dimers are detected.

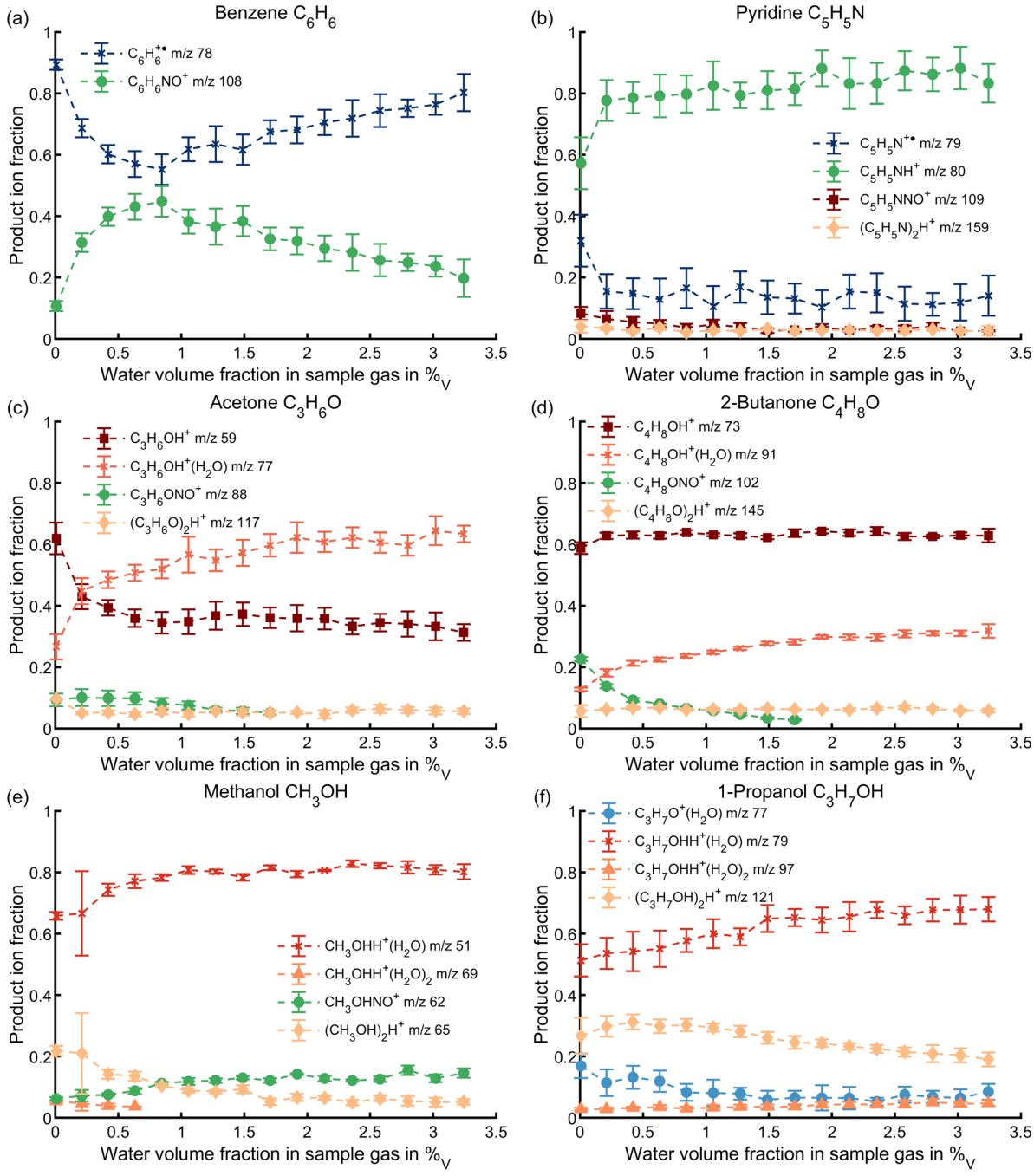

Figure 4. Product ion formation in HiKE-IMS in positive ion polarity in purified air depending on water volume fraction in the sample gas at a reduced electric field strength of 50 Td. Product ion fraction of (a) benzene, (b) pyridine, (c) acetone, (d), 2-butanone, (e) methanol, and (f) 1-propanol, each with a volume fraction of 2 ppm_V. Product ion fractions are determined by normalizing the peak area of the specific product ion to the total integral of all product ions formed by the specific analyte. The error bars show the standard deviation of ten individual measurements with the same sample. All other parameters are listed in Table 1.

Product Ion Formation at 120 Td

As can be seen from Figure 3, when operating HiKE-IMS at water volume fractions below ϕ_{H2O} = 4200 ppm_V and high E/N of 120 Td, $O_2^{+\bullet}$ is the most abundant reactant ion. Under these conditions, the reaction system is thus dominated by charge transfer. Accordingly, the product ion fractions for the various analytes at E/N = 120 Td in Figure 5 show that the precursor radical cation $M^{+\bullet}$ is the most abundant product ion for benzene (m/z 78) and pyridine (m/z 79) at water volume fractions below ϕ_{H2O} = 4200 ppm_V. Instead, the ketones acetone and 2-butanone form an ion with m/z 43, which is possibly a fragment $C_2H_3O^+$ formed by elimination of a methyl group from acetone and an ethyl group

from the radical cation of 2-butanone. In a selected ion flow tube mass spectrometry (SIFT-MS) study of ketones, the same product ion was found to be formed in reactions with $O_2^{+\bullet}$ and NO^+.[46,47] Spesyvyi et al.[46] have detected the precursor radical cations and the fragment $C_2H_3O^+$ for both acetone and 2-butanone. They have shown that fragmentation of the precursor radical cation of acetone is strongly favored by elevated ion-neutral interaction energies. In SIFDT-MS, for NO^+ and acetone at an interaction energy of 0.47 eV, the fragment accounts for about 70 % of the product ions, while for $O_2^{+\bullet}$ and acetone at an interaction energy of 0.38 eV, the fragment accounts for about 90 % of the product ions. Calculation of the ion-neutral interaction energy for acetone with NO^+ and $O2^{+\bullet}$ using the same method as Spesyvyi et al.[46,48] yields smaller interaction energies of 0.07 eV and 0.24 eV for NO^+ at 50 Td and 120 Td, respectively, and 0.06 eV and 0.16 eV for $O2^{+\bullet}$ at 50 Td and 120 Td. Compared with the SIFDT-MS study, where both the precursor radical cation and the fragment $C_2H_3O^+$ are detected, HiKE-IMS only yields the fragment $C_2H_3O^+$. A possible explanation might be a more efficient stabilization of the nascent excited adduct $(MNO^+)^*$ and the excited precursor radical cation $(M^{+\bullet})^*$ by collisions with the helium bath gas atoms present in SIFDT-MS, preventing these excited ions from dissociation, as is otherwise the case in HiKE-IMS.

In addition, 1-propanol forms a fragment identified as CH_3O^+ (*m*/*z* 31), which was also found in a SIFT-MS study of alcohols resulting from a reaction with $O_2^{+\bullet}$.[49] In addition, methanol forms the ion CH_3O^+ (*m*/*z* 31) and 1-propanol forms the ion $C_3H_7O^+$ (*m*/*z* 59), both having a mass-to-charge ratio of 1 Da below the molar mass of the neutral molecules of 32 $gmol^{-1}$ and 60 $gmol^{-1}$. Presumably, these ions $(M-H)^+$ are formed via hydride ion abstraction from the parent molecule. In SIFT-MS, CH_3O^+ (*m*/*z* 31) in the case of methanol was found to originate from a reaction with $O_2^{+\bullet}$, while $C_3H_7O^+$ (*m*/*z* 59) in the case of 1-propanol was found to be formed in a reaction with NO^+.[49] Unlike in these SIFT-MS studies, the precursor radical cation $M^{+\bullet}$ was not found in HiKE-IMS for both alcohols and both ketones, as the charge transfer with $O_2^{+\bullet}$ appears to cause fragmentation of the product ions due to the large difference in ionization energy between ΔIE = 1.85 eV for O_2 and 1-propanol and ΔIE = 2.55 eV for O_2 and 2-butanone. In contrast, the precursor radical cations of benzene and pyridine seem to be stabilized by the aromatic ring preventing their fragmentation.[50]

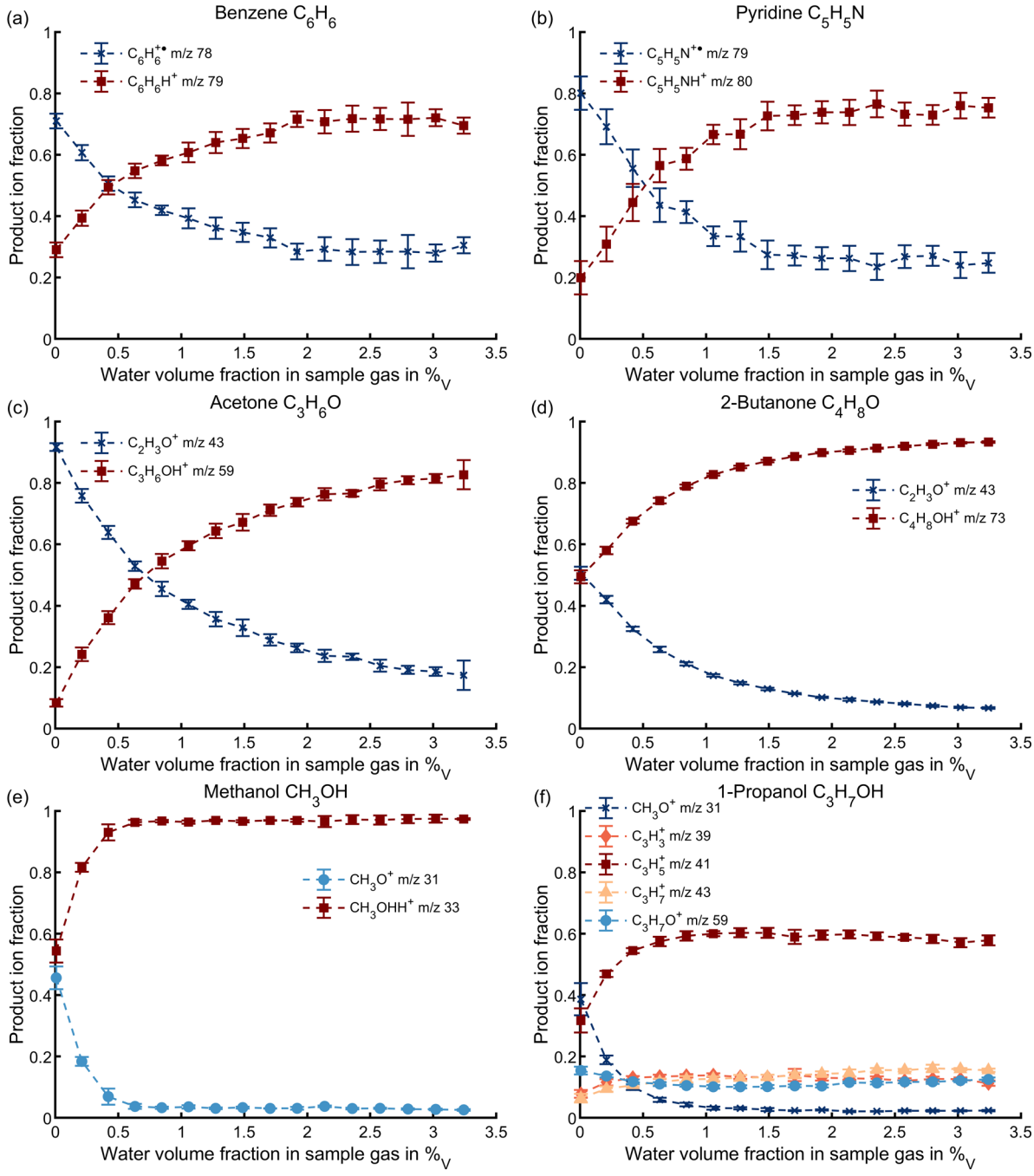

Figure 5. Product ion formation in HiKE-IMS in positive ion polarity in purified air depending on water volume fraction in the sample gas at a reduced electric field strength of 120 Td. Product ion fraction of (a) benzene, (b) pyridine, (c) acetone, (d), 2-butanone, (e) methanol, and (f) 1-propanol, each with a volume fraction of 2 ppm_V. Product ion fractions are determined by normalizing the peak area of the specific product ion to the total integral of all product ions formed by the specific analyte. The error bars show the standard deviation of ten individual measurements the same sample. All other parameters are listed in Table 1.

In contrast to the aforementioned product ions resulting from reactions with $O_2^{+\bullet}$ and NO^+, the protonated monomers account for only a small fraction of the product ions under dry conditions corresponding to ϕ_{H2O} = 70 ppm_V for most of the analytes. However, when increasing the sample gas humidity and $O_2^{+\bullet}$ is converted to H_3O^+, proton transfer dominates the reaction system again. Thus, the product ion fraction of the product ions associated with $O_2^{+\bullet}$ decreases, whereas the product ion fraction of the protonated monomers increases. In particular, the product ion fraction of CH_3O^+ (*m/z* 31) formed by both methanol and 1-propanol decreases rapidly when increasing sample gas humidity, following the same trend as the relative abundance of $O_2^{+\bullet}$, strongly indicating that the ions are formed

by charge transfer with $O_2^{+\bullet}$. Similar behavior can be seen for $C_2H_3O^+$ (*m*/*z* 43) in the case of acetone and 2-butanone. At 120 Td, in contrast to operation at 50 Td, ionization at high water volume fractions in the sample gas does not proceed via the hydrates $H_3O^+(H_2O)_n$ but via the bare H_3O^+ ions, so that all investigated analytes even those having low PA can be ionized by proton transfer even at a water volume fraction of ϕ_{H2O} = 32000 ppm_V corresponding to RH = 75% at 303.15 K and 1013.25 hPa. Clusters of the product ions with neutral molecules, such as hydrates, proton-bound dimers, and the adducts MNO^+ dissociate due to the high kinetic energies of the ions at 120 Td, making the protonated monomer the most abundant product ion. The only analyte that does not form the protonated monomer in this study is 1-propanol, which forms three fragments with *m*/*z* 43, *m*/*z* 41, and *m*/*z* 39 instead. Identical fragments were also found to be dominant product ions of 1-propanol in a study of alcohols in a proton transfer reaction mass spectrometer (PTR-MS) and were identified as $C_3H_7^+$, $C_3H_5^+$, and $C_3H_3^+$ respectively.[51] These are formed via the elimination of H_2O from the protonated monomer and subsequent elimination of H_2. Thus, unlike the reaction with the hydrates $H_3O^+(H_2O)_n$ forming $MH^+(H_2O)_x$, as those occurring in conventional IMS, the reaction of 1-propanol with H_3O^+ only yields fragments of the protonated parent molecules at 120 Td.

Besides H_3O^+, analytes can still be ionized via NO^+ even at the highest water volume fraction of ϕ_{H2O} = 32000 ppm_V when operating HiKE-IMS at 120 Td. Accordingly, 1-propanol forms the product ion $(M\text{-}H)^+$ with a constant product ion fraction of 15 – 20 %, further indicating that it is formed in reactions with NO^+, as also found in SIFT-MS.[49] Therefore, both NO^+ and $O_2^{+\bullet}$ appear to ionize alcohols via hydride ion abstraction. For benzene, the precursor radical cation and the protonated monomer approximately have the same product ion fractions at the highest water volume fraction of ϕ_{H2O} = 32000 ppm_V. Also, for pyridine, the precursor radical cation makes up for a significant fraction of about 40 % of the product ions at a water volume fraction of ϕ_{H2O} = 32000 ppm_V. Thus, supported by the reaction enthalpies for charge transfer with NO^+ and the experiment at 50 Td, both benzene and pyridine appear to react with NO^+ via charge transfer.

In general, the shift in product ion population from product ions formed by $O_2^{+\bullet}$ via charge transfer to product ions formed by bare H_3O^+ via proton transfer behaves similarly to the characteristic shift in reactant ion population when increasing water volume fraction at 120 Td and can thus indicate which reactant ions are involved in the formation of particular product ions.

Ionization Yield Depending on Sample Gas Humidity

Up to now, only the relative abundances and thus changes in the composition of the product ion population with varying water volume fractions in the sample gas have been investigated. However, for the analysis of analytes in IMS, the absolute intensity, or the ionization yield depending on sample gas humidity is also of interest. As discussed in the Introduction, increasing the humidity in conventional IMS operated at ambient pressure results in an increasing cluster size of the reactant ions $H_3O^+(H_2O)_n$ and can significantly reduce the signal intensity and even completely suppress the signal for aromatics, alcohols, and ketones.[14,15] To address whether the operation of HiKE-IMS at intermediate to high *E*/*N* can mitigate this negative influence of increased sample gas humidity on signal intensities, the ionization yield, i.e. the sum of peak areas for all product ions formed by a single analyte at given water volume fraction are shown in Figure 6. For better comparability between the different analytes, the integrals are normalized to the integral under dry conditions referring to ϕ_{H2O} = 70 ppm_V. The absolute peak areas of all product ions formed by each analyte are shown in Figures S8 and S9 for 50 Td and 120 Td, respectively.

At 50 Td, it is evident that the ionization yield of benzene and methanol, in particular, decreases as the sample gas humidity is increased. At 50 Td, benzene can only react with NO^+, which is, however, converted to $H_3O^+(H_2O)_n$ at high water volume fractions. As shown in Figure 4 and supported by the reaction enthalpies for proton transfer and ligand switching, benzene does not react with $H_3O^+(H_2O)_n$

for n ≥ 1. Correspondingly, the ionization yield of benzene rapidly decreases to about 50 % of the ionization yield under dry conditions when the water volume fraction is increased from ϕ_{H2O} = 70 ppm_V to just ϕ_{H2O} = 4200 ppm_V. Figure S8 shows that above ϕ_{H2O} = 4200 ppm_V, the sum of peak areas of all product ions formed by benzene is about 8 to 10 times lower than the sum of peak areas for all other analytes except for methanol. As shown by the reaction enthalpies in the Supporting Information, for methanol, ligand switching via $H_3O^+(H_2O)_n$ with $n \geq 2$ is endothermic, resulting in a decrease in the ionization yield above ϕ_{H2O} = 4200 ppm_V. Ultimately, at the highest water volume fraction of ϕ_{H2O} = 32000 ppm_V corresponding to RH = 75% at 303.15 K and 1013.25 hPa, the ionization yield for methanol decreases to 50 % of the ionization yield under dry conditions. While this decrease in ionization yield for both methanol and benzene is significant, it is important to emphasize that the water volume fractions used in this work are significantly higher than the water volume fractions of several 100 ppm_V where some conventional IMS are no longer able to ionize alcohols and aromatic hydrocarbons.[14,15] The remaining analytes show no decrease in ionization yield when the water volume fraction is increased. On the contrary, acetone, and 1-propanol even show a slight increase in the ionization yield of 10 % and 20 %, respectively, when increasing water volume fraction from ϕ_{H2O} = 70 ppm_V up to ϕ_{H2O} = 32000 ppm_V. The SIFT-MS studies of ketones and alcohols have shown that the proton transfer reaction with H_3O^+ proceeds with a higher reaction rate coefficient than the reactions with NO^+ and $O_2^{+\bullet}$, partly explaining the increase in signal response for acetone and 1-propanol.[47,49]

At *E*/*N* = 120 Td, no analyte shows a significant decrease in ionization yield with increasing sample gas humidity. On the contrary, the ionization yield for most analytes increases as the water volume fraction increases. Remarkably, the ionization yield for methanol, which has shown a decrease in ionization yield at high water volume fractions when the HiKE-IMS is operated at 50 Td, even increases at high water volume fractions when operating the HiKE-IMS at 120 Td. Again, this might be explained by the higher reaction rate coefficient for proton transfer with H_3O^+ than for reactions with NO^+ and $O_2^{+\bullet}$.[49] In addition, ionization of methanol at 120 Td proceeds via the bare H_3O^+ instead of its hydrates and is hence not inhibited by the otherwise gradual increase in cluster size. Also, benzene shows a slight increase in the ionization yield when increasing the water volume fraction from ϕ_{H2O} = 70 ppm_V up to ϕ_{H2O} = 4200 – 6300 ppm_V. When further increasing the water volume fraction, the ionization yield slightly decreases until at ϕ_{H2O} = 32000 ppm_V it is approximately equal to the ionization yield under dry conditions. Possibly, the initial increase is also caused by the higher reaction rate coefficient of proton transfer with H_3O^+ compared to the charge transfer with $O_2^{+\bullet}$ and NO^+.[52] The slightly declining number of formed product ions at high water volume fractions might be caused by the partial formation of the monohydrate of H_3O^+, slightly inhibiting the ionization of the analytes. However, as benzene does not react with the hydrates of H_3O^+, the bare H_3O^+ must still be present in significant amounts in the reaction region at ϕ_{H2O} = 32000 ppm_V corresponding to RH = 75% at 303.15 K and 1013.25 hPa, allowing for the ionization and thus detection of analytes with low proton affinity above the proton affinity of water with PA(H_2O) = 691 kJ/mol. Furthermore, Figure S9 shows that the sum of peak areas of all product ions is in the same order of magnitude for all analytes. Beyond that, Figures S8 and S9 show that when increasing *E*/*N* from 50 Td to 120 Td, the peak area of the most abundant product ion increase. Kirk et al. have shown that the ion current density at the end of a reaction region connected to a corona ionization source increases quadratically with increasing *E*/*N*.[20] Accordingly, the increased number of reactant ions more than compensates for the decreasing reaction time at high *E*/*N* in terms of the number of formed product ions and thus the sensitivity. Thus, operating HiKE-IMS at 120 Td not only allows for the ionization of a broad range of substances, but is also the operating point at which HiKE-IMS in most cases exhibit the optimum sensitivity.

Note that Figure 6 shows the ionization yield including all product ions formed by the specific analyte. For some analytes, the number of different product ion species formed may change as the sample gas

humidity is varied, e.g., when the reactions of 1-propanol with H_3O^+ result in the formation of multiple fragments occurring simultaneously as known for alcohols in PTR-MS.[51] This competing ionization may result in a decrease in the peak intensities of the individual product ions, even though the total number of formed product ions remains constant, simply because the constant amount of formed product ions are distributed among a larger number of possible product ion species. However, Figures S8 and S9 show that despite fragmentation of 1-propanol at E/N = 120 Td, the peak area of the most abundant product ion ($C_3H_5^+$, m/z 41) is still larger than the peak area of the most abundant product ion at E/N = 50 Td ($C_3H_7OHH^+(H_2O)$, m/z 79) by a factor of 2 – 3, depending on sample gas humidity.

In summary, when operating HiKE-IMS at E/N = 120 Td, increasing the water volume fraction in the sample gas is beneficial to the ionization yield for most of the analytes investigated in this work. Even at intermediate E/N of 50 Td, the typical negative impact of increased water volume fraction on ionization yield and sensitivity is small compared to conventional IMS operated at ambient pressure. Thus, in the context of possible field applications of HiKE-IMS, it might even be useful to intentionally increase the sample gas humidity or, as has been the approach in previous publications, to add a constant amount of water vapor to the corona ionization source in order to shift the ion chemistry into the proton transfer dominated region and thus to reduce the complexity of the ion mobility spectra recorded with HiKE-IMS.[19,30] In addition, the measurements in this work have shown that above a water volume fraction about ϕ_{H2O} = 15000 ppm_V in the sample gas, the product ion population shows no significant changes with small changes in sample gas humidity, as is conversely the case when dry sample gas is used due to the conversion of $O_2^{+\bullet}$ to $H_3O^+(H_2O)_n$.

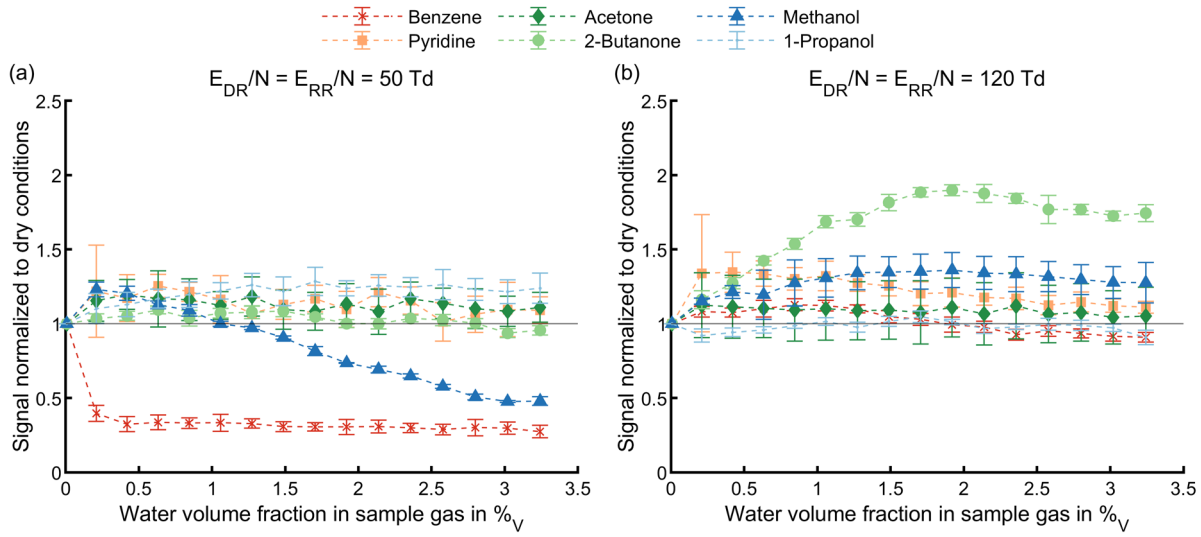

Figure 6. Integral of product ions of the investigated analytes in purified air in positive ion polarity depending on water volume fraction in the sample gas at a reduced electric field strength of a) 50 Td and b) 120 Td. The sum of integrals of the formed product ions is normalized to the sum of integrals of the formed product ions at dry conditions referring to ϕ_{H2O} = 70 ppm_V. Each analyte has a volume fraction of 2 ppm_V. The error bars show the standard deviation of ten individual measurements with the same sample. All other parameters are listed in Table 1.

The results of this work and previous works regarding the reactant ion formation and product ion formation in positive ion polarity of HiKE-IMS are summarized in the simplified reaction scheme shown in Scheme 1. In general, two systems of different reaction pathways can be involved in product ion formation in HiKE-IMS. On the one hand, analytes can be ionized via charge transfer with NO^+ and $O_2^{+\bullet}$, as well as adduct formation with NO^+. On the other hand, analytes can be ionized via proton transfer and ligand switching with the (hydrated) hydronium ions. Also, the reactions with both $O_2^{+\bullet}$ and H_3O^+ can cause fragmentation of the product ions. The conversion between these two reaction systems is caused by the conversion of the reactant ions $O_2^{+\bullet}$ and NO^+ due to hydration and subsequent reaction with neutral water molecules to form hydrated hydronium ions. Therefore, ionization via the hydrated

hydronium ions dominates at low *E*/*N* as well as at high *E*/*N* when operated at elevated sample gas humidity. In contrast, at high *E*/*N* under dry conditions, the collision-induced cluster dissociation of $O_2^{+\bullet}(H_2O)$ and $NO^+(H_2O)_3$ shifts the reaction system to ionization via charge transfer and adduct formation with NO^+. Note that under certain conditions, e.g. at 120 Td and a water volume fraction of ϕ_{H2O} = 4200 ppm_V, all reactant ions can be present simultaneously due to incomplete conversion of $O_2^{+\bullet}$ to H_3O^+ and thus be involved in product ion formation simultaneously.

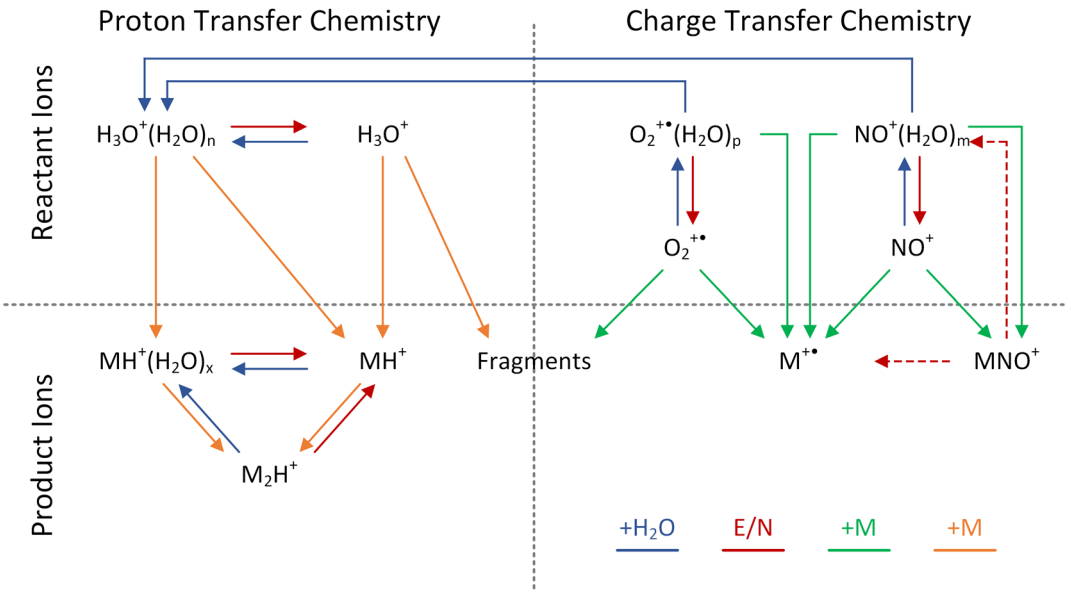

Scheme 1. Simplified reaction scheme for the formation of positive reactant ions and product ions in HiKE-IMS in purified air. The blue lines show reactions with water molecules, the red lines show reactions initiated at high E/N, and the green and orange lines show reactions with neutral analyte molecules via $NO^+(H_2O)_m$ and $O_2^{+\bullet}$, and via $H_3O^+(H_2O)_n$, respectively. The dashed red line indicates possible dissociation pathways for the adduct of the neutral analyte and NO^+.

Conclusion

In this work, we investigated the product ion formation of several model substances in HiKE-IMS depending on water volume fraction in the sample gas. The results show that the reaction system is dominated by proton transfer and ligand switching with hydrated hydronium ions at intermediate *E*/*N* of 50 Td as known from conventional IMS. However, collision-induced cluster dissociation of the reactant ions already reduces the negative effect of increasing sample gas humidity on signal intensities for most analytes. At high *E*/*N* of 120 Td, increasing the sample gas humidity shifts the ion chemistry from a charge transfer dominated reaction system at low water volume fractions to a proton transfer dominated reaction system at high water volume fractions. In contrast to conventional IMS operated at ambient pressure, all investigated analytes can be detected in HiKE-IMS when operated at high *E*/*N* without significant loss in ionization yield at high water volume fractions of up to 32000 ppm_V corresponding to RH = 75% at 303.15 K and 1013.25 hPa due to the formation of bare H_3O^+ ions. In fact, increasing the water volume fraction is even beneficial for the ionization yield of most analytes investigated in this work.

This work, along with previous works, has shown that *E*/*N* and humidity in the reaction region of HiKE-IMS influence the formed product ions. Depending on these parameters, different reactant ions are present in HiKE-IMS simultaneously and the analytes can thus be ionized through different reactions, forming multiple product ions per analyte. On the one hand, the presence of multiple product ions with their abundances depending on *E*/*N* and humidity complicates qualitative studies of product ion formation and quantitative studies of reaction kinetics. For such fundamental studies of ion chemistry in the gas phase at high effective temperatures to be conducted in HiKE-IMS, a modified ion source

providing only a single reactant ion species for the reaction region is under development. On the other hand, the presence of multiple product ions for a single analyte, especially when accompanied by a unique fragmentation pattern, can help to identify the analyte and thus to reduce false positives.

Associated Content

Supporting Information

Schematic of the gas mixing system; Ion mobility spectra and mass spectra recorded in *Selected-Mobility mode* for acetone; Ion mobility spectra and mass spectra recorded in *Selected-Mobility mode* for 2-butanone; Relative abundances of acetone depending on E_{RR}/N at E_{DR}/N = 60 Td; Relative abundances of acetone depending on E_{RR}/N at E_{DR}/N = 120 Td; Relative abundances of 2-butanone depending on E_{RR}/N at E_{DR}/N = 60 Td; Relative abundances of 2-butanone depending on E_{RR}/N at E_{DR}/N = 120 Td; Reaction enthalpies for proton transfer with $H_3O^+(H_2O)$; reaction enthalpies for ligand switching with $H_3O^+(H_2O)$; reaction enthalpies for charge transfer with $NO^+(H_2O)$ and $O_2^{+\bullet}$

Author Information

Corresponding Author

*Fax: +49 511 762 3917
E-mail: schaefer@geml.uni-hannover.de

Author Contributions

C.S. and F.S. performed the experiments. C.S. performed the data analysis. S.Z. and A.T.K. gave scientific and conceptual advice. S.Z. supervised the research project. All authors contributed to discussions and the manuscript.

Notes

The authors declare no competing financial interest.

Acknowledgements

Funded by the Deutsche Forschungsgemeinschaft (DFG, German Research Foundation) – 318063177 and 390583968.

References

(1) Eiceman, G.A., Karpas, Z., Hill, H.H.: Ion mobility spectrometry, 3rd ed., CRC Press, Boca Raton (2013)

(2) Borsdorf, H., Mayer, T., Zarejousheghani, M., Eiceman, G.A.: Recent Developments in Ion Mobility Spectrometry, *Appl. Spectrosc. Rev.*, **46**, 472–521, (2011)

(3) Kirk, A.T., Küddelsmann, M.J., Bohnhorst, A., Lippmann, M., Zimmermann, S.: Improving Ion Mobility Spectrometer Sensitivity through the Extended Field Switching Ion Shutter, *Anal. Chem*., **92**, 4838-4847, (2020)

(4) Shahin, M.M.: Mass-Spectrometric Studies of Corona Discharges in Air at Atmospheric Pressures, *J. Chem. Phys*., **45**, 2600, (1966)

(5) Pavlik, M., Skalny, J.D.: Generation of [H3O]+.(H2O)n clusters by positive corona discharge in air, *Rapid Commun. Mass Spectrom*., **11**, 1757–1766, (1997)

(6) Kim, S.H., Betty, K.R., Karasek, F.W.: Mobility behavior and composition of hydrated positive reactant ions in plasma chromatography with nitrogen carrier gas, *Anal. Chem*., **50**, 2006–2012, (1978)

(7) Sabo, M., Matejčík, Š.: Corona discharge ion mobility spectrometry with orthogonal acceleration time of flight mass spectrometry for monitoring of volatile organic compounds, *Anal. Chem*., **84**, 5327–5334, (2012)

(8) Howard, C.J.: Kinetics and Mechanism of the Formation of Water Cluster Ions from O[sub 2]+] and H2O, *J. Chem. Phys*., **57**, 3491, (1972)

(9) Fehsenfeld, F.C., Mosesman, M., Ferguson, E.E.: Ion—Molecule Reactions in an O 2 +–H 2 O System, *J. Chem. Phys*., **55**, 2115–2120, (1971)

(10) Raksit, A.B.: Reactions of O2+, O4+ and O2+·H2O ions with neutral molecules, *Int. J. Mass Spectrom. Ion Process*., **69**, 45–65, (1986)

(11) French, M.A., Hills, L.P., Kebarle, P.: Kinetics and Temperature Dependence of the Hydration of NO + in the Gas Phase, *Can. J. Chem*., **51**, 456–461, (1973)
(12) Borsdorf, H., Neitsch, K., Eiceman, G.A., Stone, J.A.: A comparison of the ion chemistry for mono-substituted toluenes and anilines by three methods of atmospheric pressure ionization with ion mobility spectrometry, *Talanta*, **78**, 1464–1475, (2009)
(13) Sabo, M., Matejčík, Š.: A corona discharge atmospheric pressure chemical ionization source with selective NO(+) formation and its application for monoaromatic VOC detection, *Analyst*, **138**, 6907–6912, (2013)
(14) Borsdorf, H., Fiedler, P., Mayer, T.: The effect of humidity on gas sensing with ion mobility spectrometry, *Sens. Actuators B Chem.*, **218**, 184–190, (2015)
(15) Safaei, Z., Willy, T.J., Eiceman, G.A., Stone, J.A., Sillanpää, M.: Quantitative response in ion mobility spectrometry with atmospheric pressure chemical ionization in positive polarity as a function of moisture and temperature, *Anal. Chim. Acta*, **1092**, 144–150, (2019)
(16) Sunner, J., Nicol, G., Kebarle, P.: Factors determining relative sensitivity of analytes in positive mode atmospheric pressure ionization mass spectrometry, *Anal. Chem*., **60**, 1300–1307, (1988)
(17) Safaei, Z., Eiceman, G.A., Puton, J., Stone, J.A., Nasirikheirabadi, M., Anttalainen, O., Sillanpää, M.: Differential Mobility Spectrometry of Ketones in Air at Extreme Levels of Moisture, *Sci. Rep.*, **9**, 5593, (2019)
(18) Kuklya, A., Uteschil, F., Kerpen, K., Marks, R., Telgheder, U.: Effect of the humidity on analysis of aromatic compounds with planar differential ion mobility spectrometry, *Int. J. Ion Mobil. Spec*., **18**, 67–75, (2015)
(19) Langejürgen, J., Allers, M., Oermann, J., Kirk, A.T., Zimmermann, S.: High kinetic energy ion mobility spectrometer: quantitative analysis of gas mixtures with ion mobility spectrometry, *Anal. Chem*., **86**, 7023–7032, (2014)
(20) Kirk, A.T., Kobelt, T., Spehlbrink, H., Zimmermann, S.: A Simple Analytical Model for Predicting the Detectable Ion Current in Ion Mobility Spectrometry Using Corona Discharge Ionization Sources, *J. Am. Soc. Mass Spectrom*., **29**, 1425–1430, (2018)
(21) Schlottmann, F., Kirk, A.T., Allers, M., Bohnhorst, A., Zimmermann, S.: High Kinetic Energy Ion Mobility Spectrometry (HiKE-IMS) at 40 mbar, *J. Am. Soc. Mass Spectrom*., **31**, 1536–1543, (2020)
(22) Borsdorf, H., Eiceman, G.A.: Ion Mobility Spectrometry: Principles and Applications, *Appl. Spectrosc. Rev*., **41**, 323–375, (2006)
(23) Gabelica, V., Marklund, E.: Fundamentals of ion mobility spectrometry, *Curr. Opin. Chem. Biol*., **42**, 51–59, (2018)
(24) Wannier, G.H.: Motion of Gaseous Ions in Strong Electric Fields, *Bell Syst. Tech. J*., **32**, 170–254, (1953)
(25) Gouw, J. de, Warneke, C., Karl, T., Eerdekens, G., van der Veen, Carina, Fall, R.: Sensitivity and specificity of atmospheric trace gas detection by proton-transfer-reaction mass spectrometry, *Int. J. Mass Spectrom*., **223-224**, 365–382, (2003)
(26) Lau, Y.K., Ikuta, S., Kebarle, P.: Thermodynamics and kinetics of the gas-phase reactions H3O+(H2O)n-1 + water = H3O+(H2O)n, *J. Am. Chem. Soc*., **104**, 1462–1469, (1982)
(27) Warneke, C., van der Veen, C, Luxembourg, S., de Gouw, J. A, Kok, A.: Measurements of benzene and toluene in ambient air using proton-transfer-reaction mass spectrometry: calibration, humidity dependence, and field intercomparison, *Int. J. Mass Spectrom*., **207**, 167–182, (2001)
(28) Allers, M., Kirk, A.T., Roßbitzky, N. von, Erdogdu, D., Hillen, R., Wissdorf, W., Benter, T., Zimmermann, S.: Analyzing Positive Reactant Ions in High Kinetic Energy Ion Mobility Spectrometry (HiKE-IMS) by HiKE-IMS-MS, *J. Am. Soc. Mass Spectrom*., **31**, 812-821, (2020)

(29) Allers, M., Kirk, A.T., Eckermann, M., Schaefer, C., Erdogdu, D., Wissdorf, W., Benter, T., Zimmermann, S.: Positive Reactant Ion Formation in High Kinetic Energy Ion Mobility Spectrometry (HiKE-IMS), *J. Am. Soc. Mass Spectrom*., **31**, 1291–1301, (2020)
(30) Langejürgen, J., Allers, M., Oermann, J., Kirk, A.T., Zimmermann, S.: Quantitative detection of benzene in toluene- and xylene-rich atmospheres using high-kinetic-energy ion mobility spectrometry (IMS), *Anal. Chem*., **86**, 11841–11846, (2014)
(31) Schaefer, C., Allers, M., Kirk, A.T., Schlottmann, F., Zimmermann, S.: Influence of Reduced Field Strength on Product Ion Formation in High Kinetic Energy Ion Mobility Spectrometry (HiKE-IMS), *J. Am. Soc. Mass Spectrom*., **32**, 1810–1820, (2021)
(32) Ellis, A.M., Mayhew, C.A.: Proton transfer reaction mass spectrometry: Principles and applications, John Wiley & Sons, Ltd, Chichester, UK (2014)
(33) Allers, M., Kirk, A.T., Schaefer, C., Schlottmann, F., Zimmermann, S.: Formation of positive product ions from substances with low proton affinity in High Kinetic Energy Ion Mobility Spectrometry (HiKE-IMS), *Rapid Commun. Mass Spectrom*., **35**, e8998, (2020)
(34) Linstrom, P.: NIST Chemistry WebBook, NIST Standard Reference Database 69, National Institute of Standards and Technology (1997)
(35) Weiss, F., Schaefer, C., Ruzsanyi, V., Märk, T.D., Eiceman, G., Mayhew, C.A., Zimmermann, S.: High kinetic energy Ion Mobility Spectrometry – Mass spectrometry investigations of four inhalation anaesthetics: Isoflurane, enflurane, sevoflurane and desflurane, *Int. J. Mass Spectrom*., 475, 116831, (2022)
(36) Smith, D., Španěl, P.: Selected ion flow tube mass spectrometry (SIFT-MS) for on-line trace gas analysis, *Mass Spectrom Rev*, **24**, 661–700, (2005)
(37) Smith, D., Wang, T., Španěl, P.: A SIFT study of the reactions of H2ONO+ ions with several types of organic molecules, *Int. J. Mass Spectrom*., **230**, 1–9, (2003)
(38) Allers, M., Schaefer, C., Ahrens, A., Schlottmann, F., Hitzemann, M., Kobelt, T., Zimmermann, S., Hetzer, R.: Detection of Volatile Toxic Industrial Chemicals with Classical Ion Mobility Spectrometry and High-Kinetic Energy Ion Mobility Spectrometry, *Anal. Chem*., **94**, 1211–1220, (2022)
(39) Kirk, A.T., Grube, D., Kobelt, T., Wendt, C., Zimmermann, S.: A High Resolution High Kinetic Energy Ion Mobility Spectrometer Based on a Low-Discrimination Tristate Ion Shutter, *Anal. Chem.,* **90**, 5603-5611, (2018)
(40) Spangler, G.E., Carrico, J.P.: Membrane inlet for ion mobility spectrometry (plasma chromatography), *Int. J. Mass Spectrom. Ion Phys*., **52**, 267–287, (1983)
(41) Španěl, P., Smith, D.: Dissociation of H3O+, NO+ and O2+• reagent ions injected into nitrogen carrier gas in SIFT-MS and reactivity of the ion fragments, *Int. J. Mass Spectrom*., **458**, 116438, (2020)
(42) Keesee, R.G., Castleman, A.W.: Thermochemical Data on Gas-Phase Ion-Molecule Association and Clustering Reactions, *J. Phys. Chem. Ref. Data*, **15**, 1011, (1986)
(43) Hiraoka, K., Takimoto, H., Morise, K.: Gas-phase hydration reactions of protonated alcohols. Energetics and bulk hydration of cluster ions, *J. Am. Chem. Soc*., **108**, 5683–5689, (1986)
(44) Valadbeigi, Y., Ilbeigi, V., Michalczuk, B., Sabo, M., Matejcik, S.: Effect of Basicity and Structure on the Hydration of Protonated Molecules, Proton-Bound Dimer and Cluster Formation: An Ion Mobility-Time of Flight Mass Spectrometry and Theoretical Study, *J. Am. Soc. Mass Spectrom*., **30**, 1242–1253, (2019)
(45) Kawai, Y., Yamaguchi, S., Okada, Y., Takeuchi, K., Yamauchi, Y., Ozawa, S., Nakai, H.: Reactions of protonated water clusters H+(H2O)n (n=1–6) with dimethylsulfoxide in a guided ion beam apparatus, *Chem. Phys. Lett*., **377**, 69–73, (2003)
(46) Spesyvyi, A., Smith, D., Španěl, P.: Ion chemistry at elevated ion-molecule interaction energies in a selected ion flow-drift tube, *Phys. Chem. Chem. Phys.*, **19**, 31714–31723, (2017)

(47) Smith, D., Wang, T., Španěl, P.: Analysis of ketones by selected ion flow tube mass spectrometry, *Rapid Commun. Mass Spectrom*., **17**, 2655–2660, (2003)
(48) Spesyvyi, A., Smith, D., Španěl, P.: Selected Ion Flow-Drift Tube Mass Spectrometry: Quantification of Volatile Compounds in Air and Breath, *Anal. Chem.*, **87**, 12151–12160, (2015)
(49) Španěl, P., Smith, D.: SIFT studies of the reactions of H3O+, NO+ and O2+ with a series of alcohols, *Int. J. Mass Spectrom. Ion Process*., **167-168**, 375–388, (1997)
(50) Španěl, P., Smith, D.: A selected ion flow tube study of the reactions of NO + and O +2 ions with some organic molecules: The potential for trace gas analysis of air, *J. Chem. Phys*., **104**, 1893–1899, (1996)
(51) Brown, P., Watts, P., Märk, T.D., Mayhew, C.A.: Proton transfer reaction mass spectrometry investigations on the effects of reduced electric field and reagent ion internal energy on product ion branching ratios for a series of saturated alcohols, *Int. J. Mass Spectrom*., **294**, 103–111, (2010)
(52) Španěl, P., Smith, D.: Selected ion flow tube studies of the reactions of H3O+, NO+, and O2+ with several aromatic and aliphatic hydrocarbons, *Int. J. Mass Spectrom*., **181**, 1–10, (1998)

For Table of Contents Use Only

Influence of Sample Gas Humidity on Product Ion Formation in High Kinetic Energy Ion Mobility Spectrometry (HiKE-IMS)

Christoph Schaefer*, Florian Schlottmann, Ansgar T. Kirk, Stefan Zimmermann